



Oxidizing capacity of the rural atmosphere in Hong Kong, Southern China



Zeyuan Li ^a, Likun Xue ^{a,*}, Xue Yang ^a, Qiaozhi Zha ^b, Yee Jun Tham ^b, Chao Yan ^b, Peter K.K. Louie ^c, Connie W.Y. Luk ^c, Tao Wang ^b, Wenxing Wang ^a

^a Environment Research Institute, Shandong University, Ji'nan, Shandong, China

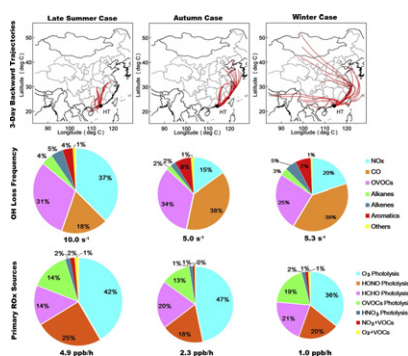
^b Department of Civil and Environmental Engineering, Hong Kong Polytechnic University, Hong Kong, China

^c Environmental Protection Department, the Government of the Hong Kong Special Administrative Region, Hong Kong, China

HIGHLIGHTS

- Well-defined seasonal patterns of AOC, k_{OH} and RO_x production were found in rural Hong Kong.
- k_{OH} was dominated by oxidation of NO_2 and OVOCs in later summer and of CO and OVOCs in autumn and winter.
- Major primary RO_x sources were photolysis of O_3 and HONO in late summer and photolysis of O_3 and HCHO in autumn and winter.

GRAPHICAL ABSTRACT



ARTICLE INFO

Article history:

Received 4 July 2017

Received in revised form 30 August 2017

Accepted 30 August 2017

Available online 8 September 2017

Editor: D. Barcelo

Keywords:

Atmospheric oxidizing capacity

OH reactivity

Radical source

Observation-based model

Southern China

ABSTRACT

Atmospheric oxidizing capacity (AOC), dominated by the hydroxyl radical (OH), is an important index of the self-cleaning capacity of atmosphere and plays a vital role in the tropospheric chemistry. To better understand the key processes governing the chemistry of rural atmosphere of southern China, we analyzed the oxidation capacity and radical chemistry at a regional background site in Hong Kong from 23 August to 22 December 2012, which covered the summer, autumn and winter seasons. A chemical box model built on the latest Master Chemical Mechanism (v3.3) was used to elucidate the OH reactivity and sources of RO_x radicals ($RO_x = OH + HO_2 + RO_2$). The AOC showed a clear seasonal pattern with stronger intensity in late summer compared to autumn and winter. Reactions with NO_2 (30%) and oxygenated volatile organic compounds (OVOCs) (31%) together dominated the OH loss in summer, while reactions with CO (38% in autumn and 39% in winter) and OVOCs (34% in autumn and 25% in winter) made larger contributions in autumn and winter. Photolysis of O_3 (36–47%) presented the major RO_x source during all three seasons. The second largest RO_x source was HONO photolysis (25% in summer compared to HCHO photolysis in autumn (20%) and winter (21%)). Besides, photolysis of other OVOCs was another important primary source of RO_x radicals with average contributions of 14%, 13% and 20% for the summer, autumn and winter cases, respectively. Overall, the present study evaluates the oxidizing capacity of the rural atmosphere of South China and elucidates the varying characteristics of photochemical processes in different air masses.

© 2017 Elsevier B.V. All rights reserved.

* Corresponding author.

E-mail address: xuelikun@sdu.edu.cn (L. Xue).

1. Introduction

Atmospheric oxidizing capacity (AOC) is the essential driving force of atmospheric chemistry. It determines the removal rates of most primary pollutants including carbon monoxide (CO), nitrogen oxides (NO_x), methane (CH₄) and non-methane volatile organic compounds (NMVOCs) (Elshorbany et al., 2009) as well as the production rates of secondary pollutants such as ozone (O₃) and secondary organic aerosols (SOA) (Prinn, 2003). AOC is generally defined as the sum of oxidation rates of various primary pollutants (i.e., CO, CH₄, NMVOCs) by the oxidants (i.e., OH, O₃ and NO₃ radicals) (Elshorbany et al., 2009; Xue et al., 2016). The hydroxyl radical (OH) is the central player of atmospheric chemistry, accounting for the majority of AOC, and initiates the degradation of the variety of natural and anthropogenic trace gases. The OH loss frequency (or usually referred to as OH reactivity), defined as the inverse of the OH lifetime, has been widely used as an indicator of the intensity of atmospheric oxidation and is dependent on the abundances and compositions of primary pollutants (Mao et al., 2010; Xue et al., 2016). Besides, the primary source strength of RO_x radicals (RO_x = OH + HO₂ + RO₂) determines the availability of radicals and hence the initiation of atmospheric oxidation processes. Therefore, AOC, OH reactivity, and RO_x source are three crucial aspects for understanding the complex atmospheric photochemistry.

During the recent decades, a number of studies have been carried out to investigate the atmospheric oxidizing capacity and radical chemistry over different regions of the world. For instance, detailed chemical budgets of OH and HO₂ radicals have been analyzed by sophisticated chemical box models in various metropolitan areas, such as Birmingham (Heard et al., 2004), Tokyo (Kanaya et al., 2007), London (Emmerson et al., 2007), Santiago (Elshorbany et al., 2009), Mexico City (Volkamer et al., 2010), Beijing (Liu et al., 2012) and Hong Kong (Xue et al., 2016). These efforts demonstrated the capability of current chemical models to simulate reasonably the ambient radicals and their chemistry mechanisms in the polluted atmospheres. In addition, it has been found that the primary RO_x sources mainly include photolysis of O₃, nitrous acid (HONO), formaldehyde (HCHO) and other oxygenated volatile organic compounds (OVOCs) as well as reactions of O₃ with VOCs, but the dominant radical source(s) varies largely with different regions (Volkamer et al., 2010; Xue et al., 2016). Generally, ozone photolysis and ozonolysis reactions of unsaturated VOCs are the dominant OH sources in the rural areas (Martinez et al., 2003; Volkamer et al., 2010), whilst photolysis of HONO and/or OVOCs plays a more important role in the polluted atmospheres (Ren et al., 2003; Michoud et al., 2014; Elshorbany et al., 2009; Volkamer et al., 2010; Liu et al., 2012; Emmerson et al., 2007). Furthermore, most of the previous works were performed in the heavily polluted metropolitan areas, with only a few efforts focusing on the rural atmospheres. Consequently, exploring the oxidizing capacity and radical sources in the rural background atmospheres presents a significant supplement to the understanding of atmospheric radical chemistry on a regional scale.

In recent years, China has been suffering from widespread and serious photochemical air pollution that is characterized by high concentrations of O₃, peroxyacetyl nitrate (PAN) and carbonyls (e.g., T. Wang et al., 2017; Xue et al., 2014a, 2014b; Yang et al., 2017; Zhang et al., 2015). An increasing body of research has been conducted to examine the sensitivity of O₃ formation to its precursors, based on which anti-pollution control strategies can be formulated (e.g., Zhang et al., 2008; Xue et al., 2014a). In comparison, atmospheric oxidizing capacity and radical sources, the 'core' of atmospheric chemistry, have been rarely investigated in China. Limited studies, mostly occurring in the Pearl River delta (PRD), North China Plain (NCP) and Yangtze River Delta (YRD), have confirmed the strong atmospheric oxidizing capacity in the polluted atmosphere of China, which facilitates fast oxidation of various primary pollutants and formation of O₃ and SOA (Hofzumahaus et al., 2009; Lu et al., 2012; Liu et al., 2012; Xue et al., 2016; Nan et al., 2017). More such kind of efforts are much needed to better understand the underlying chemical causes of photochemical air pollution in China.

To investigate the atmospheric oxidizing capacity and radical chemistry in the rural atmosphere of Hong Kong and the adjacent PRD region, a 4-month intensive field campaign was carried out at Hok Tsui from August to December 2012. This site is an ideal regional background station in southern China that receives various air masses including clean maritime air as well as polluted air from Hong Kong, the PRD region and eastern China (Wang et al., 1998; Wang et al., 2001a, 2001b; Wang et al., 2009). With the intensive measurement data in the present study, a detailed chemical modeling analysis was conducted to quantify the AOC, OH reactivity and radical sources in the polluted air masses of different origins. Firstly, we will show the overall observations of trace gases and the origins of polluted air masses sampled in summer, autumn and winter seasons. Then, we will analyze the intensity and chemical budget of AOC, OH reactivity, and RO_x radical sources in different types of air masses. Overall, this study can provide some new insights into the core area of atmospheric chemistry – oxidizing capacity and radical chemistry – in the rural background atmosphere of southern China, and demonstrates the different chemical signatures of regional air masses from different origins.

2. Methods

2.1. Experiments

The field measurements were performed at the Hong Kong Polytechnic University's air monitoring station at Hok Tsui (22.22°N, 114.25°E, 60 m above sea level), which is located in the southeastern tip of Hong Kong Island. The station is a typical coastal site with a 270° view of the South China Sea, and has been used as a regional background site in many previous studies. Under the influence of the Asian monsoon, this site receives contrasting air masses including clean marine air, polluted plumes from Hong Kong and the PRD region, and aged continental air masses transported from East China (Xu et al., 2015b; Wang et al., 2009). It should be noted that under the influence of tropical cyclone in summer and autumn, stagnant weather with high temperature and low humidity conditions usually causes quite serious photochemical smog episode in this region (Wang et al., 1998; Xue et al., 2016). In the present study, a 4-month measurement campaign was carried out from 23 August to 22 December 2012, which covered three distinct types of the foregoing air masses (see Fig. 2).

Ozone, HONO, NO, NO₂, CO, PAN, C₂–C₁₀ non-methane hydrocarbons, C₁–C₈ carbonyls, J_{NO2}, and meteorological parameters were simultaneously measured. The instruments and their calibration procedures have been described elsewhere (Zha et al., 2014; Xu et al., 2015a; Xue et al., 2016), and only a brief description is given here (see Table S1 in the supplementary material for a summary of measurement parameters and techniques). O₃ was measured by a commercial ultraviolet photometric instrument (TEI model 49i); HONO was measured using a long path absorption photometer (QUMA model LOPAP-03) (Zha et al., 2014); NO and NO₂ were measured by a chemiluminescence analyzer (TEI model 42i) equipped with a blue light converter (Xu et al., 2013); CO was measured by a non-dispersive infrared analyzer (API Model 300EU); PAN was measured with a custom-built thermo-dissociation chemical ionization mass spectrometer (THS Instruments Inc., Atlanta) (Tham et al., 2014; X.F. Wang et al., 2017). C₂–C₁₀ non-methane hydrocarbons were measured by a commercial analyzer combining gas chromatography with photoionization detection and flame-ionization detection (Syntech Spectras, model GC955 Series 600/800 POCP) (Xue et al., 2014b). Temperature, relative humidity (RH), and wind speed and direction were monitored by a commercial sensor (M. R. Young, Model 41382VC/VF) and a two-axis ultrasonic wind sensor (Gill Instruments, Model 1405-PK-021). Photolysis frequency of NO₂ (J_{NO2}) was measured with a filter radiometer (Meteorologie Consult gmbh). The time resolution of the data was 1-min averaged for O₃, HONO, NO, NO₂, CO, PAN, temperature, RH, J_{NO2} and wind speed and direction, and 30-min averaged for C₂–C₁₀ non-methane hydrocarbons. Furthermore, 24-hour air

samples were collected by DNPH-coated sorbent cartridges on selected days (e.g., 29 August, 10 October and 13 December), and were then subject to high pressure liquid chromatography analysis to detect C₁–C₈ carbonyls (Ho et al., 2011; Xue et al., 2014c; Yang et al., 2017).

2.2. The OBM-AOCP model

The OBM-AOCP (Observation-Based Model for investigating the Atmospheric Oxidative Capacity and Photochemistry), a zero-dimensional chemical box model, was deployed in the present study to simulate the in-situ atmospheric photochemistry and quantify the AOC, OH reactivity and RO_x budget. It has been successfully utilized in many previous studies (Xue et al., 2013; Xue et al., 2014a; Xue et al., 2014b; Xue et al., 2014c; Xue et al., 2015; Xue et al., 2016). Briefly, the model is based on the latest version of the Master Chemical Mechanism (MCM v3.3), a nearly explicit gas phase mechanism describing the degradation of 143 primarily emitted VOCs, resulting in 17,224 reactions involving 5833 molecular and free radical species (Saunders et al., 2003). In addition to the existing reactions in MCM v3.3, the heterogeneous reactions of NO₂, HO₂, NO₃, N₂O₅, ClONO₂ and HOCl were also incorporated (Xue et al., 2014a). Meanwhile, we also optimized the model with some physical processes such as the variations of boundary layer height and solar zenith angle, dry deposition, and the dilution of air pollutants within the planetary boundary layer (Xue et al., 2014a).

The OBM-AOCP is capable of explicitly computing the AOC, OH reactivity and RO_x budget. Since the radical chemistry is the core part of atmospheric chemistry, >15,000 reactions are related with the radical chemical processes in the MCM v3.3. To estimate the AOC and radical budgets, we have tracked almost all of the reactions in the MCM and individually computed their reaction rates. The AOC was calculated as the sum of reaction rates of the oxidation of CO, CH₄, alkanes, alkenes, aromatics and OVOCs by OH, O₃ and NO₃ radicals (Xue et al., 2016). The AOC contributed by the individual oxidant can be also quantified. The OH loss rate was computed by tracking and adding together the reaction rates of OH with CO, CH₄, alkanes, alkenes, aromatics, OVOCs, NO, NO₂, HONO, HNO₃, HO₂ and HO₂NO₂ (see Fig. 5). The major primary RO_x sources include photolysis of O₃, HONO, HNO₃, H₂O₂, HCHO and other OVOCs as well as the reactions of O₃ + VOCs and NO₃ + VOCs (Xue et al., 2016).

The measurement data of O₃, NO, NO₂, CO, HONO, PAN, CH₄, C₂–C₁₀ non-methane hydrocarbons, carbonyls, temperature, RH and J_{NO2} were averaged or interpolated to a time resolution of 5 min for the model constraints. The photolysis frequencies of other molecules, such as O₃, HCHO, HONO, other OVOCs, etc., were parameterized as a function of solar zenith angle in the model and further scaled by the measured J_{NO2} (Saunders et al., 2003). For carbonyls, since only 24-h data were available, the diurnal variations were first simulated with the model without carbonyl constraints and then scaled with the measured 24-hour average data. In the present study, only the most abundant carbonyl species, i.e., HCHO, CH₃CHO, C₂H₅CHO, CH₃COCH₃ and benzaldehyde, were scaled to the measurement concentrations (see Fig. S1 for the measurement-scaled diurnal profiles of carbonyls). This should be a reasonable approach to derive diurnal data of carbonyls without high resolution measurements available. Although it may introduce some uncertainty to the subsequent modeling analysis, sensitivity studies without observed carbonyl constraints showed that the major conclusions of the present study remained unchanged (see Fig. S2). Three multi-day pollution cases in late summer, autumn and winter were selected for the simulation, each of which lasted for 6 days and reflected different types of air masses. The model started from 00:00 local time (LT) and pre-run for four days with the campaign average data to approach steady state for the unconstrained compounds. The output of the final run was then subject to further analyses.

3. Results and discussion

3.1. Overview of observations

Fig. 1 shows the measured time series of air pollutants and meteorological parameters at Hok Tsui from 23 August to 22 December 2012. A distinct seasonal variation of air quality and meteorological condition can be clearly illustrated. Under the influence of the Asian monsoon, the study site generally received clean maritime air from the South China Sea in summer, leading to a hot humid weather and good air quality. At the end of summer (i.e., 23–29 August 2012), however, a distant tropical cyclone on the west Pacific ocean introduced a stagnant weather condition that favored the accumulation of air pollutants in Hong Kong and the PRD region. A drastic photochemical smog episode was observed during this period. In autumn, the air flow was dominated by transport of regional air masses from Hong Kong and the PRD region, and the weather condition was featured by relatively high temperature (with a mean value of ~26 °C) and strong solar radiation, which induced the photochemical reactions. The prevailing regional transport and warm weather make autumn to be the most polluted season when higher levels of O₃ and PAN were observed. In winter, the northeasterly monsoon was the main synoptic process, and thus the air flow was controlled by the long-range transport of aged continental air masses. The weather condition was characterized by relatively low temperature and weak solar radiation, and most air pollutants were presented at a quite low level except for the long-lived pollutants such as CO. Overall, different weather conditions and varying types of air masses were observed in different seasons, which would result in a seasonal variation in the atmospheric oxidation chemistry and air quality.

To investigate the oxidizing capacity and radical chemistry in different types of air masses, we further selected three polluted cases in late summer (23–28 August), autumn (9–14 October) and winter (9–14 December) for the detailed analyses. The daily average concentrations of various air pollutants (including VOCs) and meteorological parameters during the three cases are summarized in Table 1 (and detailed time series of the selected cases are provided in the supplement). The late summer case was marked by the highest photochemical pollution levels, with the daily maximum hourly O₃ mixing ratios exceeding 100 ppbv almost every day (except for 26 August). The peak values of O₃ and PAN were recorded at 159 ppbv and 4427 pptv, respectively. The O₃ precursors were also present at very high concentrations. For example, the maximum levels of NO_x, CO, alkenes, aromatics and alkanes were 91.5 ppbv, 470 ppbv, 4462 pptv, 4370 pptv and 7875 pptv, respectively. These observations revealed the markedly poor air quality and also implied strong atmospheric oxidative capacity over the region during this episode. The physical origin of this episode was a distant tropical cyclone which introduced a warm stagnant weather to Hong Kong and the PRD region. Under the condition of high temperature (with daytime average of 31 °C), moderate RH (daytime average of 67%) and strong solar radiation (with peak J_{NO2} of $9.3 \times 10^{-3} \text{ s}^{-1}$), the air pollutants were easily accumulated and undergone extensive photochemical reactions to produce secondary pollutants such as O₃ and PAN. The 72-hour backward trajectories arriving at Hok Tsui at an altitude of 100 m above ground level were calculated by the HYSPLIT model (Draxler and Rolph, 2016) and are shown in Fig. 2a, which suggest that most of air masses were from the upwind Hong Kong and PRD region. Therefore, this case can reflect the chemical signatures of polluted plumes from local Hong Kong and the PRD region.

During the autumn case, the maximum levels of most air pollutants were lower than those in the late summer episode, but the overall average concentrations of O₃ and CO were much higher. In comparison, the average concentration levels of O₃ precursors, i.e., NO_x and VOCs, were the lowest among the three cases (see Table 1), suggesting the transport of regional aged air masses that had undergone photochemical processing to the study site. The stable and warm weather condition, with wind speed < 2 m·s⁻¹ for most of the time and average temperature of 26 °C,

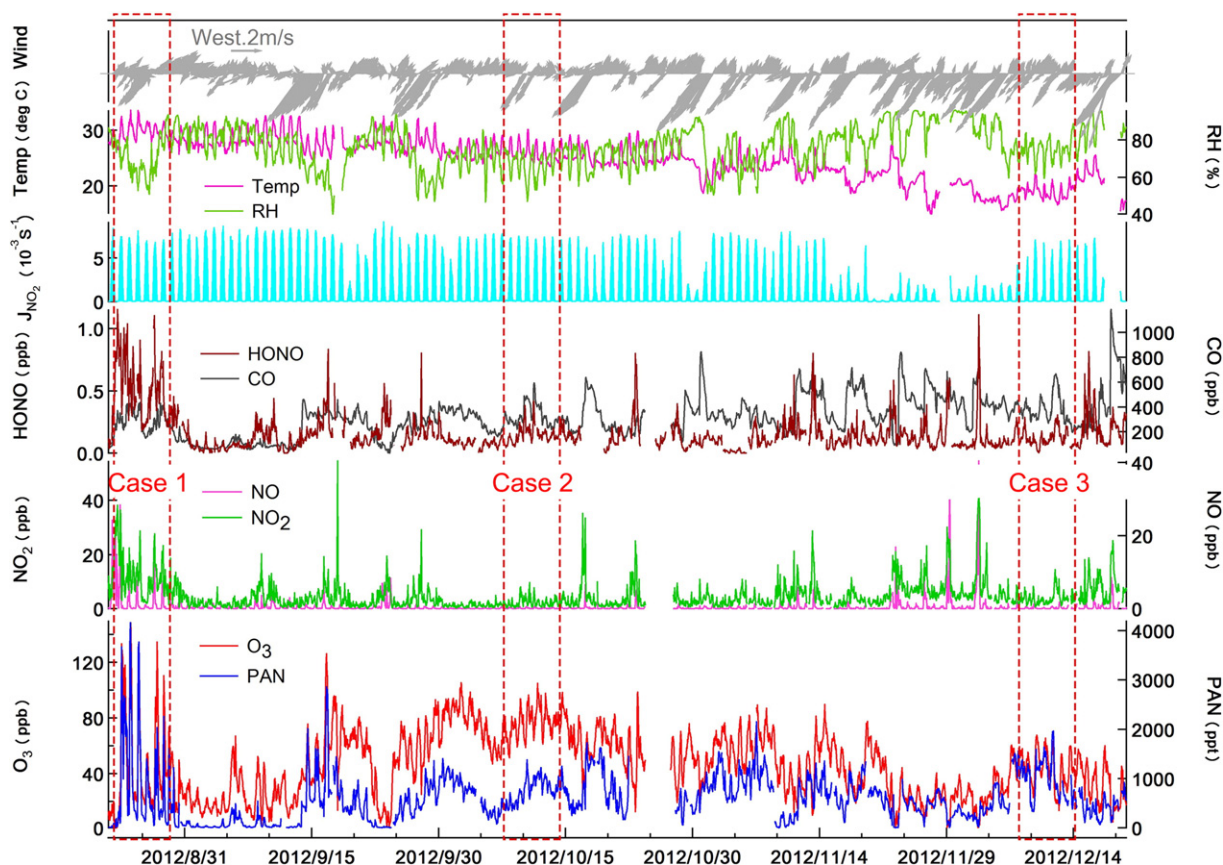


Fig. 1. Time series of air pollutants and meteorological parameters observed at Hok Tsui from 23 August to 20 December 2012. The data gaps were mainly due to the calibration and maintenance of the instruments. Three red dashed squares highlight the three polluted cases which are subject to detailed analyses.

avored the gradual accumulation of air pollutants in the autumn season (see Fig. 1). The 72-hour backward trajectories also suggested that the transport of processed air masses from Southeast China played a dominant role (Fig. 2b). Thus, this case can be deployed to investigate the photochemical processes in the aged regional plumes from Southeast China.

In comparison with the late summer and autumn cases, the winter-time case was featured by lower temperature ($19 \pm 2^\circ\text{C}$), higher RH ($75\% \pm 6\%$), slightly weaker solar radiation (with average peak J_{NO_2} of $6.0 \times 10^{-3} \text{ s}^{-1}$), and better air quality. The concentration levels of most air pollutants were the lowest during the winter case, except for the long-lived species such as CO, ethane and benzene, which showed

Table 1

Summary of the daily average concentrations and standard deviations of trace gases and meteorological parameters measured during the late summer (case 1), autumn (case 2) and winter (case 3) cases. The unit is pptv for the hydrocarbon species.

Species	Case 1	Case 2	Case 3	Species	Case 1	Case 2	Case 3
O ₃ (ppb)	51 ± 38	79 ± 11	43 ± 13	1-Butene	62 ± 123	5 ± 13	50 ± 123
CO (ppb)	298 ± 79	335 ± 89	358 ± 123	trans-2-Butene	34 ± 48	5 ± 17	24 ± 97
NO (ppb)	1.9 ± 4.3	0.1 ± 0.2	0.2 ± 0.5	cis-2-Butene	39 ± 70	4 ± 0	22 ± 91
NO ₂ (ppb)	12.2 ± 8.3	2.9 ± 2.4	4.2 ± 3.1	1,3-Butadiene	49 ± 114	6 ± 18	21 ± 65
HONO (ppb)	0.54 ± 0.25	0.16 ± 0.07	0.11 ± 0.07	1-Pentene	23 ± 42	5 ± 0	20 ± 141
PAN (ppt)	959 ± 1013	843 ± 205	918 ± 408	trans-2-Pentene	6 ± 10	5 ± 0	7 ± 37
J_{NO_2} (10^{-3} s^{-1})	2.28 ± 2.80	2.12 ± 2.78	1.56 ± 2.35	Isoprene	488 ± 604	26 ± 71	18 ± 101
Temp (°C)	29.9 ± 1.5	25.8 ± 1.6	19.2 ± 1.5	Ethyne	1246 ± 1114	1607 ± 991	1144 ± 1043
RH (%)	69.1 ± 9.6	66.8 ± 7.1	75.1 ± 6.2	Benzene	349 ± 170	478 ± 120	535 ± 233
Ethane	1862 ± 935	2934 ± 701	2450 ± 1380	Toluene	1198 ± 1075	477 ± 248	991 ± 621
Propane	1004 ± 960	513 ± 322	896 ± 579	Ethylbenzene	270 ± 250	89 ± 224	154 ± 192
n-Butane	992 ± 960	198 ± 193	365 ± 337	m/p-Xylene	328 ± 446	79 ± 220	146 ± 289
i-Butane	654 ± 608	204 ± 160	294 ± 264	o-Xylene	126 ± 185	25 ± 76	44 ± 106
n-Pentane	265 ± 277	74 ± 124	120 ± 131	1,3,5-Trimethylbenzene	5 ± 5	6 ± 0	6 ± 0
i-Pentane	471 ± 495	145 ± 233	230 ± 240	1,2,4-Trimethylbenzene	17 ± 52	7 ± 0	7 ± 0
n-Hexane	161 ± 244	104 ± 0	125 ± 0	1,2,3-Trimethylbenzene	6 ± 2	7 ± 0	8 ± 0
i-Hexane	167 ± 307	21 ± 60	113 ± 272	HCHO ^a	-	3627	1419
n-Heptane	63 ± 32	93 ± 0	160 ± 312	CH ₃ CHO ^a	-	975	523
i-Octane	267 ± 307	15 ± 57	51 ± 87	C ₂ H ₅ CHO ^a	-	39	30
n-Octane	79 ± 150	45 ± 0	50 ± 0	CH ₃ COCH ₃ ^a	-	684	179
Ethene	456 ± 363	391 ± 381	436 ± 497	Benzaldehyde ^a	-	818	552
Propene	166 ± 136	19 ± 43	175 ± 159				

^a The carbonyls data were the 24-h average concentrations based on the measurements on 10th Oct. and 13th Dec. 2012.

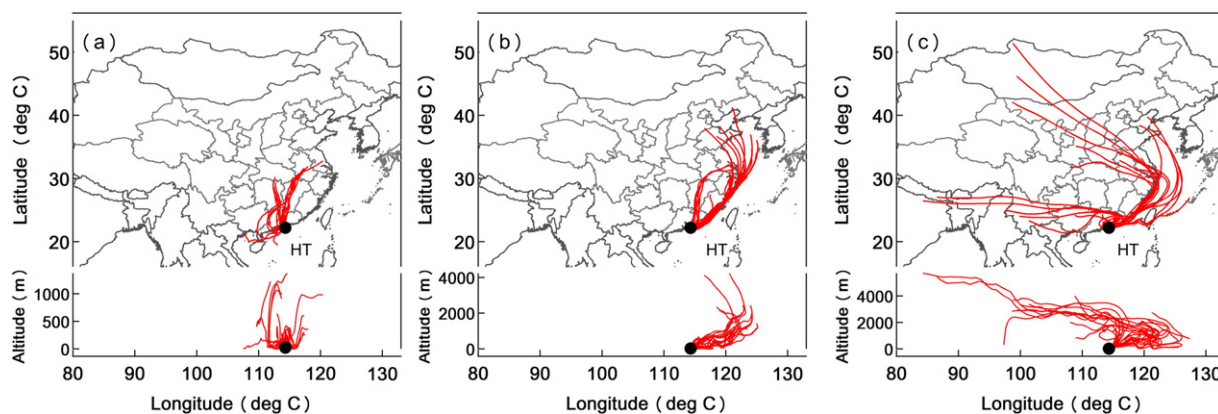


Fig. 2. Three-day backward trajectories of air masses arriving at Hok Tsui at an altitude of 100 m above ground level at 00:00 and 12:00 LT every day during (a) Case 1 (23–28 August), (b) Case 2 (9–14 October), and (c) Case 3 (9–14 December).

the highest levels (see Table 1). This was mainly due to the long-range transport of aged continental air masses under the influence of the northeasterly winter monsoons. The transported plumes had experienced adequate atmospheric photochemical reactions prior to arriving at Hok Tsui. This is further evidenced by the 72-h back trajectories as shown in Fig. 2c, which show the fast transport of continental air masses from eastern China to the study site. Overall, these three cases captured contrasting air masses and meteorological conditions in different seasons, facilitating a comprehensive investigation of atmospheric oxidizing capacity and radical chemistry in different types of atmosphere environments. In the following section, we will utilize the OBM-AOCP model to quantify the AOC, OH reactivity and ROx radical sources for these three representative cases.

3.2. Atmospheric oxidative capacity

The time series of model-calculated AOC at Hok Tsui during the three cases is shown in Fig. 3. The maximum AOC levels were up to 1.4×10^8 , 6.2×10^7 and 4.1×10^7 molecules $\text{cm}^{-3} \text{s}^{-1}$ in the late

summer, autumn and winter cases, respectively. The daytime average (06:00–19:00 LT in summer, 06:00–18:00 LT in autumn, and 06:30–18:00 LT in winter) AOC levels were 3.3×10^7 , 1.6×10^7 and 1.1×10^7 molecules $\text{cm}^{-3} \text{s}^{-1}$ for the three cases, corresponding to total numbers of 1.54×10^{12} , 6.83×10^{11} and 4.64×10^{11} molecules of CO, CH₄ and NMVOCs photochemically depleted throughout the daytime in the ambient air. Obviously, the oxidizing capacity of atmosphere was the strongest in the summer episode compared to the moderately high levels during the autumn and winter cases.

The AOC presented similar diurnal variation patterns during the three cases, with the maximum intensity at around noontime and lower levels at night. Such profiles tracked closely with the diurnal variations of solar radiation (as indicative of the J_{NO_2} in Fig. 1) and model-calculated OH radicals (figures not shown). The contributions of individual oxidants to the AOC were essentially the same for the three cases. At daytime, OH was as expected the predominant oxidant accounting for 96.8%, 98.6% and 98.1% of the AOC during the three cases, followed by NO₃ with average contributions of 1.8% (5.79×10^5 molecules $\text{cm}^{-3} \text{s}^{-1}$), 1.1% (2.26×10^5 molecules $\text{cm}^{-3} \text{s}^{-1}$) and 1.2%

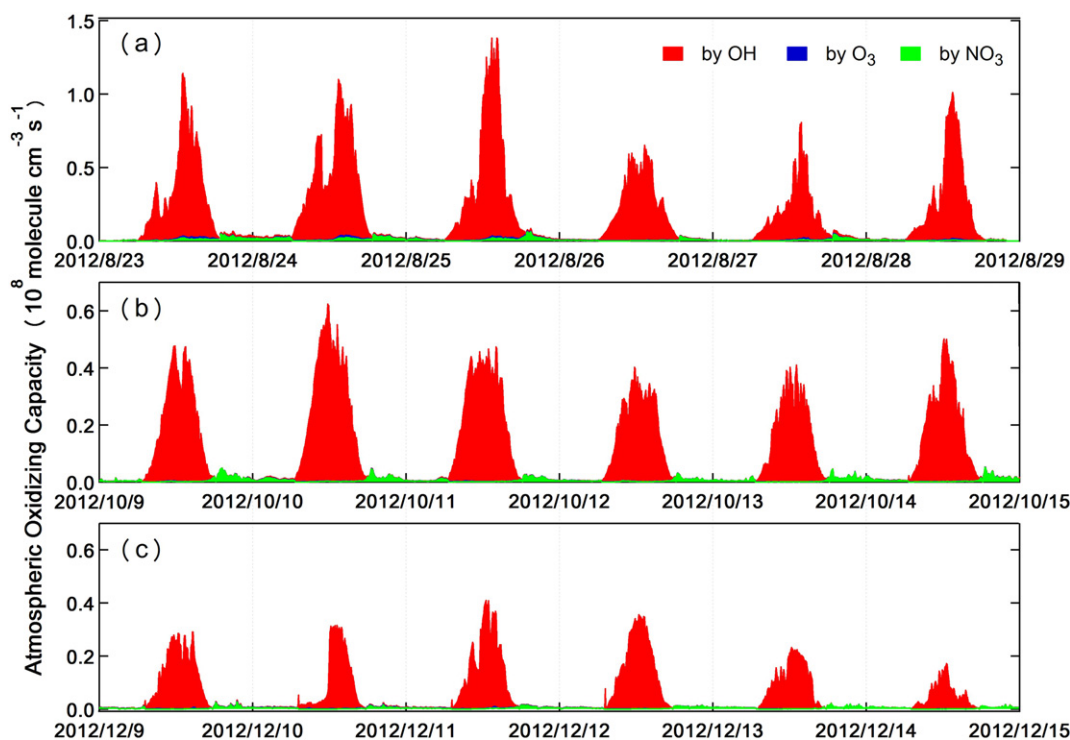


Fig. 3. The model-calculated AOC and its breakdown to the individual oxidants at Hok Tsui during (a) Case 1, (b) Case 2 and (c) Case 3.

(1.33×10^5 molecules $\text{cm}^{-3} \text{s}^{-1}$). In comparison, O_3 only presented a minor contribution (1.5%, 0.3% and 0.8%). During the nighttime, NO_3 turned over to be the major oxidant, accounting for 63.0%, 88.5% and 79.1% of the AOC, followed by OH (26.8%, 7.2% and 10.8%) and O_3 (10.3%, 4.3% and 10.2%) in the late summer, autumn and winter cases. Overall, these results are in accordance with the previous studies, which indicated that OH was the predominant oxidant and accounted for the majority of the AOC (Hofzumahaus et al., 2009). It should be noted that the reactive chlorine atom arising from photolysis of nitryl chloride may also contribute considerably to the atmospheric oxidizing capacity at Hok Tsui (Tham et al., 2014), but it was not quantified in the present study.

The AOC levels at Hok Tsui in summertime are much higher than those determined at a rural site in Germany (Geyer et al., 2001), but much lower than those derived from some polluted urban areas, such as the downtown of Santiago, Chile (Elshorbany et al., 2009) and Tung Chung, Hong Kong (Xue et al., 2016). For instance, the peak AOC levels during a severe photochemical episode at Tung Chung, a polluted urban/new town air monitoring station in western Hong Kong, were about twice higher than those at Hok Tsui (the remote coastal site in eastern Hong Kong) during the late summer episode, with the daytime average levels being even approximately six times higher at Tung Chung (Xue et al., 2016). Another interesting finding was that NO_3 showed a considerable contribution to the oxidizing capacity not only at Tung Chung but also at Hok Tsui in the afternoon during the multi-day photochemical smog episodes in summer (Xue et al., 2016), while such phenomena was not found in the autumn and winter cases.

3.3. OH reactivity

The model-calculated OH loss rates and their breakdown for the three cases are depicted in Fig. 4. Clearly, the OH loss rates were the highest in the late summer case, with an average (\pm standard deviation) value of $9.2 \pm 3.7 \text{ s}^{-1}$, compared to $4.6 \pm 1.1 \text{ s}^{-1}$ and $5.4 \pm 2.0 \text{ s}^{-1}$ in the autumn and winter cases. The maximum OH loss rates were up to 29.5 s^{-1} , 12.5 s^{-1} and 13.8 s^{-1} during the late summer, autumn and winter cases, respectively. The OH reactivity estimated at Hok Tsui

was much lower than those determined from the heavily polluted areas such as London (average value of 18.1 s^{-1} ; Whalley et al., 2016), Paris (median value of 33 s^{-1} ; Dolgorouky et al., 2012), New York (average value of 25 s^{-1} ; X.R. Ren et al., 2006), Backgarden (a rural site in the PRD region) (mean maximum value of 50 s^{-1} ; Lou et al., 2010), and Tung Chung (maximum value of 34 s^{-1} ; Xue et al., 2016), but was comparable or higher than those in Nashville ($11.3 \pm 4.8 \text{ s}^{-1}$; Kovacs et al., 2003), Whiteface Mountain, (average value of 5.6 s^{-1} ; X. Ren et al., 2006), and a mountain site in Wilmington, Pennsylvania (average value of 6.1 s^{-1} ; Ren et al., 2005). Here the estimated k_{OH} accounted for the OH oxidation of both measured species (such as NO_x , CO, C_1 – C_{10} hydrocarbons and measured carbonyls) and modeled compounds (mainly including unmeasured higher OVOCs and HNO_3). As shown in Fig. 4, the k_{OH} from the measured compounds accounted for the majority (63%–79%) of the total k_{OH} at Hok Tsui. It should be noted that the k_{OH} estimated solely from the modeled results may be subject to some uncertainty due to the lack of direct observations.

Fig. 5 shows the average diurnal profiles of OH loss rates for the three cases. Distinct diurnal variations of the OH reactivity are clearly illustrated among different cases. In the late summer case, the OH reactivity exhibited a morning peak, which was mainly contributed by the reactions of NO_x with OH. This should be ascribed to the transport of freshly emitted urban plumes from downtown Hong Kong to the study site. In the autumn case in comparison, the OH reactivity showed a broad peak in the late afternoon with the maximum level appearing at 18:00 LT. The increase of OH reactivity in the afternoon was dominated by the reactions of OH with OVOCs, which should be related to the transport of regional OVOCs-laden air masses and photochemical formation of OVOCs at daytime. During the winter case, the OH reactivity showed higher levels in the evening compared to relatively lower values during the daytime. This was mainly owing to the transport of the regional air masses containing abundant CO, NO_x and OVOCs.

Moreover, the partitioning of OH reactivity to the principal groups of reactants also varied with different cases. During the late summer episode, the OH reactivity was dominated by the reactions of OH with NO_x , with an average contribution of 37.5%, followed by the reactions with OVOCs (30.8%) and CO (17.8%). The oxidation of alkanes, alkenes

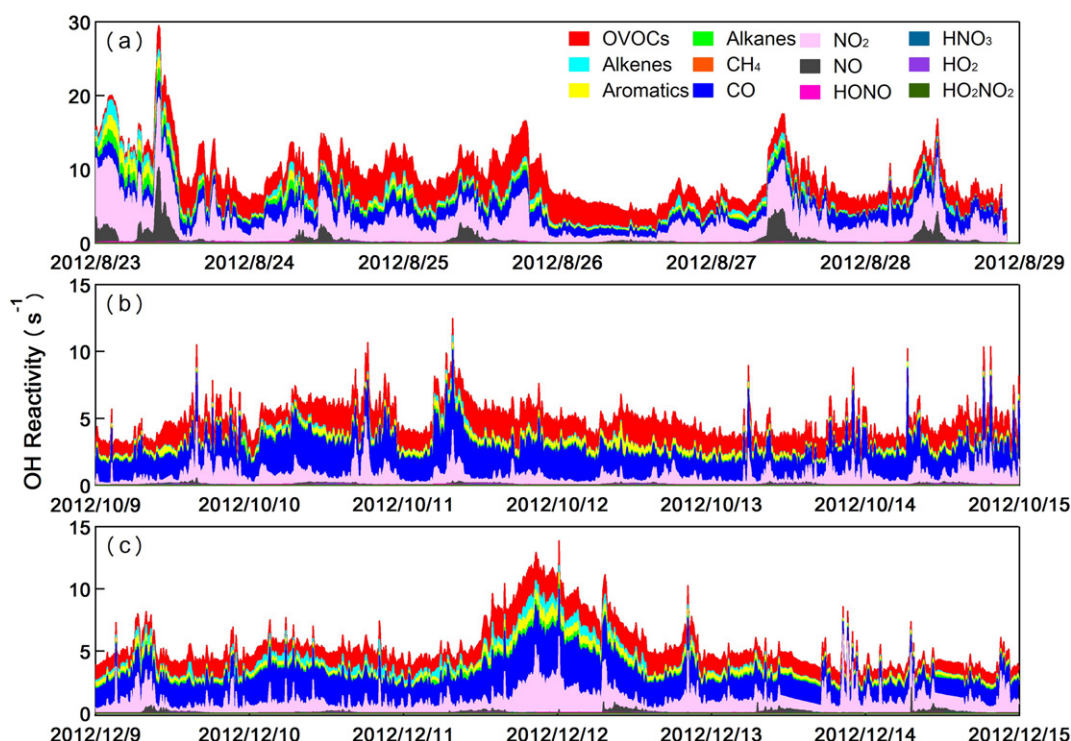


Fig. 4. The model-calculated OH reactivity and its breakdown to the major reactant groups during (a) Case 1, (b) Case 2, and (c) Case 3.

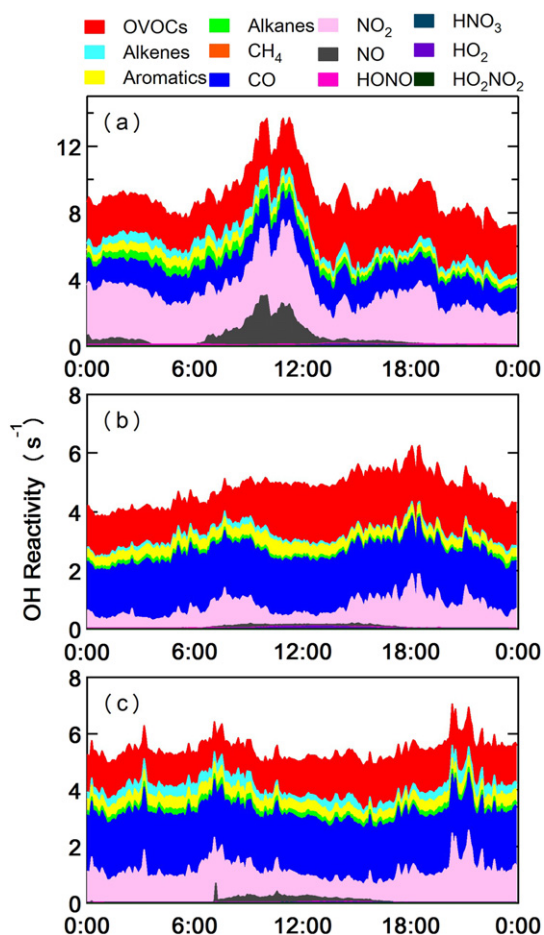


Fig. 5. Average diurnal profiles of OH reactivity in (a) Case 1, (b) Case 2, and (c) Case 3.

and aromatics accounted for on average 4.3%, 4.7% and 3.8% of the total OH reactivity, respectively. In the autumn case, the oxidation of CO by OH was the predominant contributor (38.2% on average) of the OH reactivity, followed by the reactions with OVOCs (33.6%) and NO_x (15.1%). Besides, the reactions of OH with aromatic VOCs also made an average contribution of 7.5% and played a more important role than that in the late summer case. During the winter case, the principal reactants were essentially the same to those in the autumn case. Specifically, CO, OVOCs and NO_x accounted for 38.7%, 25.4% and 20.0% of the OH reactivity. The above analysis clearly elucidates the difference in the inherent photochemical processes and major reactants in the different seasons (or different types of air masses) over southern China.

3.4. Primary RO_x sources

Table 2 documents the average contributions of the individual radical sources to the primary RO_x production for the three cases, and Fig. 6 presents the average daytime profiles of RO_x production rates from the major four source pathways. Photolysis of O₃ and HONO are major OH sources; OVOCs photolysis is principal sources of HO₂ and RO₂; and ozonolysis reactions of unsaturated VOCs can produce OH, HO₂ and RO₂ radicals. In the present study, we evaluated the primary RO_x production by considering the sources of OH, HO₂ and RO₂ equally. As expected, the primary production of RO_x radicals was the strongest during the late summer episode, followed by the autumn and winter cases. Photolysis of O₃ turned out to be the predominant RO_x source (as OH supplier) during all the three cases, with average contributions of 41.6%, 46.7% and 35.7%, respectively. However, the relative

Table 2

Daytime average contributions of major primary RO_x sources for the three cases.

Major sources	Case 1	Case 2	Case 3
O ₃ photolysis	41.6%	46.7%	35.7%
HONO photolysis	24.7%	17.9%	19.7%
HCHO photolysis	14.6%	20.3%	21.0%
OVOCs photolysis	14.3%	12.5%	19.5%
HNO ₃ photolysis	1.8%	1.5%	1.7%
NO ₃ + VOCs	1.6%	0.7%	1.3%
O ₃ + VOCs	1.4%	0.3%	1.0%

contributions of the other radical sources varied among different cases. In the late summer case, HONO photolysis was the second largest source with an average contribution of 24.7%, followed by the photolysis of HCHO (14.6%) and other OVOCs (14.3%). In comparison, photolysis of HCHO presented the second most important radical source in the autumn (20.3%) and winter cases (21.0%), followed by photolysis of HONO (17.9% in autumn and 19.7% in winter) and other OVOCs (12.5% in autumn and 19.5% in winter). The higher contribution from HONO photolysis in the late summer case was mainly attributed to the higher concentrations of HONO (see Fig. S6) and stronger solar irradiation compared to the autumn and winter cases. A recent study also observed elevated concentrations of HONO in late summer at a suburban site in western Hong Kong, and suggested a significant unknown daytime HONO source (Xu et al., 2015a). However, exploring the potential unknown sources of daytime HONO is beyond the scope of the present study. Other recognized radical sources, such as photolysis of HNO₃ and H₂O₂, ozonolysis reactions of unsaturated VOCs, and reactions of NO₃ with VOCs, generally presented a minor negligible contribution (<2%) in all three cases.

The above analysis reveals that photolysis of O₃, HONO, HCHO and other OVOCs were the major primary RO_x sources at Hok Tsui, yet their relative contributions varied case by case. This is consistent with the previous studies that showed a significant variation of atmospheric radical sources among different places (Volkamer et al., 2010; Stone et al., 2012). Recently, Xue et al. (2016) analyzed the radical chemistry during a severe photochemical smog episode in the late August of 2011 at Tung Chung, a polluted receptor site in western Hong Kong, and found that photolysis of OVOCs was the predominant radical source. Besides, photolysis of HONO, O₃ and HCHO were the other important radical sources, while ozonolysis reactions of unsaturated VOCs and reactions of NO₃ with VOCs also presented considerable contributions to the primary RO_x production at Tung Chung. Such budget of radical source is obviously distinct with those we derived at Hok Tsui in the present study, which showed the dominant role of O₃ photolysis. This difference should be attributed to the difference in the chemical environments of Tung Chung and Hok Tsui, and clearly reflects the large heterogeneity in the radical sources, which may vary significantly with place (even in a small area) and time (e.g., different seasons).

4. Summary

We demonstrate in the present study the seasonal variation of atmospheric oxidizing capacity, OH reactivity, and primary RO_x sources, three essential aspects of atmospheric chemistry, in the rural atmosphere of Hong Kong, southern China. Three polluted cases occurring in late summer, autumn and winter seasons, representing different types of air masses, were carefully selected for an in-depth modeling analysis. The strongest AOC, OH reactivity and primary RO_x production were determined in late summer compared to autumn and winter. During the late summer case with the influence of polluted urban plumes from Hong Kong and the RPD region, the reactions with NO_x and OVOCs dominated the OH loss, and photolysis of O₃ and HONO were the major radical sources. For the autumn and winter cases under the

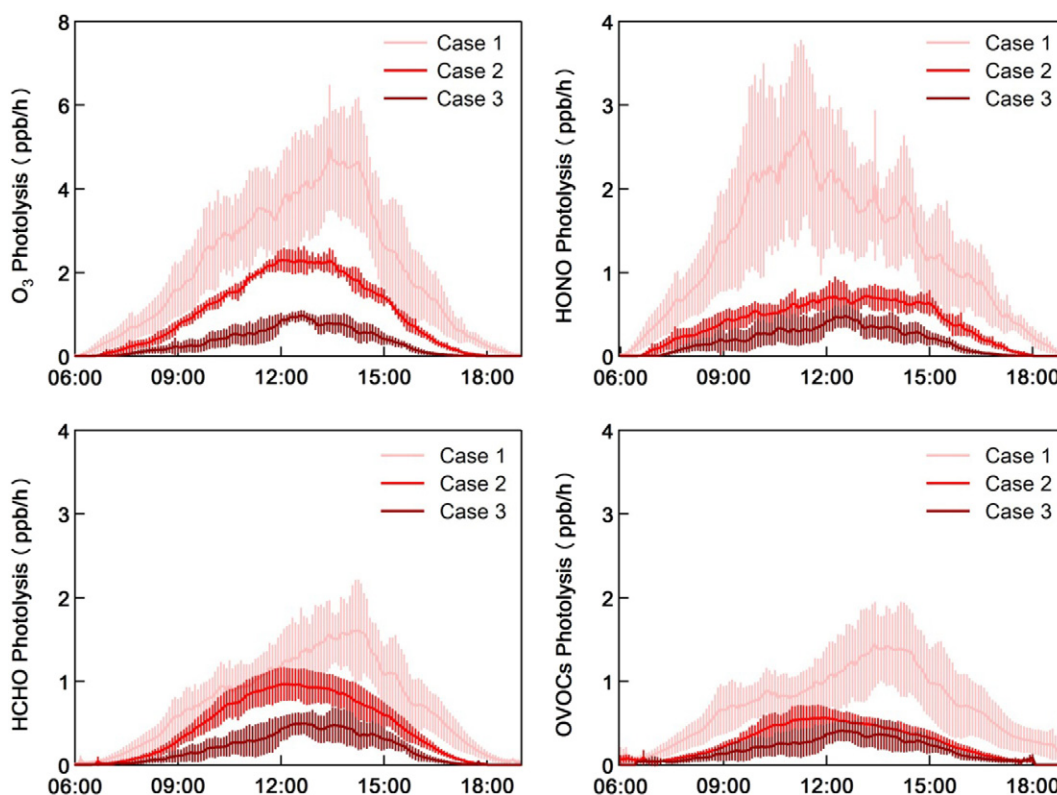


Fig. 6. Daytime average profiles of the ROx radical production rates from photolysis of O₃, HONO, HCHO and OVOCs during the three cases. The error bars represent the standard deviations.

influences of aged regional and super-regional air masses from eastern China, the reactions with CO and OVOCs contributed to the majority of the OH reactivity, and photolysis of O₃ and HCHO dominated the primary ROx production. This study clearly elucidates the significant variations in the chemical oxidation processes in different atmospheric environments.

Acknowledgements

The authors thank Steven Poon and Much Yeung for their contributions to the field study. We are also grateful to the NOAA Air Resources Laboratory for providing the HYSPLIT model and to the University of Leeds for providing the Master Chemical Mechanism (v3.3). This work was funded by the National Natural Science Foundation of China (project number: 41505111), the National Key Research and Development Programme of the Ministry of Science and Technology of China (2016YFC0200503), the Qilu Youth Talent Programme of Shandong University, and the Jiangsu Collaborative Innovation Center for Climate Change. The field measurement data used in this study were collected with support from the Hong Kong Environmental Protection Department, Hong Kong Environmental Conservation Fund, and the Hong Kong Research Grants Council.

Disclaimer

The opinions expressed in this paper are those of the authors and do not necessarily reflect the views or policies of the Government of the Hong Kong Special Administrative Region, nor does mention of trade names or commercial products constitute an endorsement or recommendation of their use.

Appendix A. Supplementary data

Supplementary data to this article can be found online at <http://dx.doi.org/10.1016/j.scitotenv.2017.08.310>.

References

- Dolgorouky, C., Gros, V., Sarda-Estevé, R., Sinha, V., Williams, J., Marchand, N., Sauvage, S., Poulain, L., Sciare, J., Bonsang, B., 2012. Total OH reactivity measurements in Paris during the 2010 MEGAPOLI winter campaign. *Atmos. Chem. Phys.* 12, 9593–9612.
- Draxler, R., Rolph, G., 2016. HYSPLIT (HYbrid Single-Particle Lagrangian Integrated Trajectory) Model Access via NOAA ARLREADY Website. <http://ready.arl.noaa.gov/HYSPLIT.php> (last access: 26 May 2016). NOAA Air Resources Laboratory, Silver Spring, MD.
- Elshorbany, Y.F., Kurtenbach, R., Wiesen, P., Lissi, E., Rubio, M., Villena, G., Gramsch, E., Rickard, A.R., Pilling, M.J., Kleffmann, J., 2009. Oxidation capacity of the city air of Santiago, Chile. *Atmos. Chem. Phys.* 9, 2257–2273.
- Emmerson, K.M., Carslaw, N., Carslaw, D.C., Lee, J.D., McFiggans, G., Bloss, W.J., Gravesstock, T., Heard, D.E., Hopkins, J., Ingham, T., Pilling, M.J., Smith, S.C., Jacob, M., Monks, P.S., 2007. Free radical modelling studies during the UK TORCH campaign in summer 2003. *Atmos. Chem. Phys.* 7, 167–181.
- Geyer, A., Alicke, B., Konrad, S., Schmitz, T., Stutz, J., Platt, U., 2001. Chemistry and oxidation capacity of the nitrate radical in the continental boundary layer near Berlin. *J. Geophys. Res.-Atmos.* 106 (D8), 8013–8025.
- Heard, D.E., Carpenter, L.J., Creasey, D.J., Hopkins, J.R., Lee, J.D., Lewis, A.C., Pilling, M.J., Seakins, P.W., Carslaw, N., Emmerson, K.M., 2004. High levels of the hydroxyl radical in the winter urban troposphere. *Geophys. Res. Lett.* 31 (18).
- Ho, S.S.H., Ho, K.F., Liu, W.D., Lee, S.C., Dai, W.T., Cao, J.J., Ip, H.S.S., 2011. Unsuitability of using the DNPH-coated solid sorbent cartridge for determination of airborne unsaturated carbonyls. *Atmos. Environ.* 45, 261–265.
- Hofzumahaus, A., Rohrer, F., Lu, K.D., Bohn, B., Brauers, T., Chang, C.C., Fuchs, H., Holland, F., Kita, K., Kondo, Y., Li, X., Lou, S.R., Shao, M., Zeng, L.M., Wahner, A., Zhang, Y.H., 2009. Amplified trace gas removal in the troposphere. *Science* 324, 1702–1704.
- Kanaya, Y., Cao, R.Q., Akimoto, H., Fukuda, M., Komazaki, Y., Yokouchi, Y., Koike, M., Tanimoto, H., Takegawa, N., Kondo, Y., 2007. Urban photochemistry in central Tokyo: 1. Observed and modeled OH and HO₂ radical concentrations during the winter and summer of 2004. *J. Geophys. Res.-Atmos.* 112 (D21).
- Kovacs, T.A., Brune, W.H., Harder, H., Martinez, M., Simpas, J.B., Frost, G.J., Williams, E., Jobson, T., Stroud, C., Young, V., Fried, A., Wert, B., 2003. Direct measurements of urban OH reactivity during Nashville SOS in summer 1999. *J. Environ. Monit.* 5, 68–74.
- Liu, Z., Wang, Y., Gu, D., Zhao, C., Huey, L.G., Stickel, R., Liao, J., Shao, M., Zhu, T., Zeng, L., Amoroso, A., Costabile, F., Chang, C.C., Liu, S.C., 2012. Summertime photochemistry during CAREBeijing-2007: ROx budgets and O₃ formation. *Atmos. Chem. Phys.* 12, 7737–7752.
- Lou, S., Holland, F., Rohrer, F., Lu, K., Bohn, B., Brauers, T., Chang, C.C., Fuchs, H., Haseler, R., Kita, K., Kondo, Y., Li, X., Shao, M., Zeng, L., Wahner, A., Zhang, Y., Wang, W., Hofzumahaus, A., 2010. Atmospheric OH reactivities in the Pearl River Delta - China in summer 2006: measurement and model results. *Atmos. Chem. Phys.* 10, 11243–11260.

- Lu, K.D., Rohrer, F., Holland, F., Fuchs, H., Bohn, B., Brauers, T., Chang, C.C., Häseler, R., Hu, M., Kita, K., Kondo, Y., Li, X., Lou, S.R., Nehr, S., Shao, M., Zeng, L.M., Wahner, A., Zhang, Y.H., Hofzumahaus, A., 2012. Observation and modelling of OH and HO₂ concentrations in the Pearl River Delta 2006: a missing OH source in a VOC-rich atmosphere. *Atmos. Chem. Phys.* 12, 1541–1569.
- Mao, J.Q., Ren, X.R., Chen, S.A., Brune, W.H., Chen, Z., Martinez, M., Harder, H., Lefer, B., Rappengluck, B., Flynn, J., Leuchner, M., 2010. Atmospheric oxidation capacity in the summer of Houston 2006: comparison with summer measurements in other metropolitan studies. *Atmos. Environ.* 44, 4107–4115.
- Martinez, M., Harder, H., Kovacs, T.A., Simpas, J.B., Bassis, J., Leshner, R., Brune, W.H., Frost, G.J., Williams, E.J., Stroud, C.A., Jobson, B.T., Roberts, J.M., Hall, S.R., Shetter, R.E., Wert, B., Fried, A., Alicke, B., Stutz, J., Young, V.L., White, A.B., Zamora, R.J., 2003. OH and HO₂ concentrations, sources, and loss rates during the southern oxidants study in Nashville, Tennessee, summer 1999. *J. Geophys. Res.-Atmos.* 108 (D19).
- Michoud, V., Colomb, A., Borbon, A., Miet, K., Beekmann, M., Camredon, M., Aumont, B., Perrier, S., Zapf, P., Siour, G., Ait-Helal, W., Afif, C., Kukui, A., Furger, M., Dupont, J.C., Haefelin, M., Doussin, J.F., 2014. Study of the unknown HONO daytime source at a European suburban site during the MEGAPOLI summer and winter field campaigns. *Atmos. Chem. Phys.* 14, 2805–2822.
- Nan, J., Wang, S., Guo, Y., Xiang, Y., Zhou, B., 2017. Study on the daytime OH radical and implication for its relationship with fine particles over megacity of Shanghai, China. *Atmos. Environ.* 154, 167–178.
- Prinn, R.G., 2003. The cleansing capacity of the atmosphere. *Annu. Rev. Environ. Resour.* 28, 29–57.
- Ren, X.R., Harder, H., Martinez, M., Leshner, R.L., Olinger, A., Shirley, T., Adams, J., Simpas, J.B., Brune, W.H., 2003. HO_x concentrations and OH reactivity observations in New York City during PMTACS-NY2001. *Atmos. Environ.* 37, 3627–3637.
- Ren, X.R., Brune, W.H., Cantrell, C.A., Edwards, G.D., Shirley, T., Metcalf, A.R., Leshner, R.L., 2005. Hydroxyl and peroxy radical chemistry in a rural area of Central Pennsylvania: observations and model comparisons. *J. Atmos. Chem.* 52, 231–257.
- Ren, X., Brune, W.H., Olinger, A., Metcalf, A.R., Simpas, J.B., Shirley, T., Schwab, J.J., Bai, C., Roychowdhury, U., Li, Y., Cai, C., Demerjian, K.L., He, Y., Zhou, X., Gao, H., Hou, J., 2006. OH, HO₂, and OH reactivity during the PMTACS-NY Whiteface Mountain 2002 campaign: observations and model comparison. *J. Geophys. Res.-Atmos.* 111 (D10).
- Ren, X.R., Brune, W.H., Mao, J.Q., Mitchell, M.J., Leshner, R.L., Simpas, J.B., Metcalf, A.R., Schwab, J.J., Cai, C.X., Li, Y.Q., Demerjian, K.L., Felton, H.D., Boynton, G., Adams, A., Perry, J., He, Y., Zhou, X.L., Hou, J., 2006. Behavior of OH and HO₂ in the winter atmosphere in New York city. *Atmos. Environ.* 40, S252–S263.
- Saunders, S.M., Jenkin, M.E., Derwent, R.G., Pilling, M.J., 2003. Protocol for the development of the master chemical mechanism, MCM v3 (part a): tropospheric degradation of non-aromatic volatile organic compounds. *Atmos. Chem. Phys.* 3, 161–180.
- Stone, D., Whalley, L.K., Heard, D.E., 2012. Tropospheric OH and HO₂ radicals: field measurements and model comparisons. *Chem. Soc. Rev.* 41, 6348–6404.
- Tham, Y.J., Yan, C., Xue, L.K., Zha, Q.Z., Wang, X.F., Wang, T., 2014. Presence of high nitril chloride in Asian coastal environment and its impact on atmospheric photochemistry. *Chin. Sci. Bull.* 59 (4), 356–359.
- Volkamer, R., Sheehy, P., Molina, L.T., Molina, M.J., 2010. Oxidative capacity of the Mexico City atmosphere - part 1: a radical source perspective. *Atmos. Chem. Phys.* 10, 6969–6991.
- Wang, T., Lam, K.S., Lee, A.S.Y., Pang, S.W., Tsui, W.S., 1998. Meteorological and chemical characteristics of the photochemical ozone episodes observed at Cape D'Aguiar in Hong Kong. *J. Appl. Meteorol.* 37, 1167–1178.
- Wang, T., Cheung, V.T.F., Lam, K.S., Kok, G.L., Harris, J.M., 2001a. The characteristics of ozone and related compounds in the boundary layer of the South China coast: temporal and vertical variations during autumn season. *Atmos. Environ.* 35, 2735–2746.
- Wang, T., Wu, Y.Y., Cheung, T.F., Lam, K.S., 2001b. A study of surface ozone and the relation to complex wind flow in Hong Kong. *Atmos. Environ.* 35, 3203–3215.
- Wang, T., Wei, X.L., Ding, A.J., Poon, C.N., Lam, K.S., Li, Y.S., Chan, L.Y., Anson, M., 2009. Increasing surface ozone concentrations in the background atmosphere of Southern China, 1994–2007. *Atmos. Chem. Phys.* 9, 6217–6227.
- Wang, T., Xue, L.K., Brimblecombe, P., Lam, Y.F., Li, L., Zhang, L., 2017. Ozone pollution in China: a review of concentrations, meteorological influences, chemical precursors, and effects. *Sci. Total Environ.* 575, 1582–1596.
- Wang, X.F., Wang, T., Xue, L.K., Nie, W., Xu, Z., Poon, C.N., Wang, W.X., 2017. Peroxyacetyl nitrate measurements by thermal dissociation–chemical ionization mass spectrometry in an urban environment: performance and characterizations. *Front. Environ. Sci. Eng.* 11 (4), 1–8.
- Whalley, L.K., Stone, D., Bandy, B., Dunmore, R., Hamilton, J.F., Hopkins, J., Lee, J.D., Lewis, A.C., Heard, D.E., 2016. Atmospheric OH reactivity in central London: observations, model predictions and estimates of in situ ozone production. *Atmos. Chem. Phys.* 16, 2109–2122.
- Xu, Z., Wang, T., Xue, L.K., Louie, P.K.K., Luk, C.W.Y., Gao, J., Wang, S.L., Chai, F.H., Wang, W.X., 2013. Evaluating the uncertainties of thermal catalytic conversion in measuring atmospheric nitrogen dioxide at four differently polluted sites in China. *Atmos. Environ.* 76, 221–226.
- Xu, Z., Wang, T., Wu, J.Q., Xue, L.K., Chan, J., Zha, Q.Z., Zhou, S.Z., Louie, P.K.K., Luk, C.W.Y., 2015a. Nitrous acid in a polluted subtropical atmosphere: seasonal variability, direct vehicle emission, and heterogeneous production on ground. *Atmos. Environ.* 106, 100–109.
- Xu, Z., Xue, L.K., Wang, T., Xia, T., Gao, Y., Louie, P.K.K., Luk, C.W.Y., 2015b. Measurements of peroxyacetyl nitrate at a background site in the Pearl River Delta Region: production efficiency and regional transport. *Aerosol Air Qual. Res.* 15, 833–841.
- Xue, L.K., Wang, T., Guo, H., Blake, D.R., Tang, J., Zhang, X.C., Saunders, S.M., Wang, W.X., 2013. Sources and photochemistry of volatile organic compounds in the remote atmosphere of western China: results from the Mt. Waliguan observatory. *Atmos. Chem. Phys.* 13, 8551–8567.
- Xue, L.K., Wang, T., Gao, J., Ding, A.J., Zhou, X.H., Blake, D.R., Wang, X.F., Saunders, S.M., Fan, S.J., Zuo, H.C., Zhang, Q.Z., Wang, W.X., 2014a. Ground-level ozone in four Chinese cities: precursors, regional transport and heterogeneous processes. *Atmos. Chem. Phys.* 14, 13175–13188.
- Xue, L.K., Wang, T., Louie, P.K.K., Luk, C.W.Y., Blake, D.R., Xu, Z., 2014b. Increasing external effects negate local efforts to control ozone air pollution: a case study of Hong Kong and implications for other Chinese cities. *Environ. Sci. Technol.* 48, 10769–10775.
- Xue, L.K., Wang, T., Wang, X.F., Blake, D.R., Gao, J., Nie, W., Gao, R., Gao, X.M., Xu, Z., Ding, A.J., Huang, Y., Lee, S.C., Chen, Y.Z., Wang, S.L., Chai, F.H., Zhang, Q.Z., Wang, W.X., 2014c. On the use of an explicit chemical mechanism to dissect peroxy acetyl nitrate formation. *Environ. Pollut.* 195, 39–47.
- Xue, L.K., Saunders, S.M., Wang, T., Gao, R., Wang, X.F., Zhang, Q.Z., Wang, W.X., 2015. Development of a chlorine chemistry module for the master chemical mechanism. *Geosci. Model Dev.* 8, 3151–3162.
- Xue, L.K., Gu, R.R., Wang, T., Wang, X.F., Saunders, S.M., Blake, D.R., Louie, P.K.K., Luk, C.W.Y., Simpson, I.J., Xu, Z., 2016. Oxidative capacity and radical chemistry in the polluted atmosphere of Hong Kong and Pearl River Delta region: analysis of a severe photochemical smog episode. *Atmos. Chem. Phys.* 16, 9891–9903.
- Yang, X., Xue, L., Yao, L., Li, Q., Wen, L., Zhu, Y., Chen, T., Wang, X., Yang, L., Wang, T., Lee, S., Chen, J., Wang, W., 2017. Carbonyl compounds at Mount Tai in the North China plain: characteristics, sources, and effects on ozone formation. *Atmos. Res.* 196, 53–61.
- Zha, Q.Z., Xue, L.K., Wang, T., Xu, Z., Yeung, C., Louie, P.K.K., Luk, C., 2014. Large conversion rates of NO₂ to HNO₂ observed in air masses from the South China Sea: evidence of strong production at sea surface? *Geophys. Res. Lett.* 41, 7710–7715.
- Zhang, Y.H., Su, H., Zhong, L.J., Cheng, Y.F., Zeng, L.M., Wang, X.S., Xiang, Y.R., Wang, J.L., Gao, D.F., Shao, M., Fan, S.J., Liu, S.C., 2008. Regional ozone pollution and observation-based approach for analyzing ozone-precursor relationship during the PRIDE-PRD2004 campaign. *Atmos. Environ.* 42, 6203–6218.
- Zhang, G., Mu, Y.J., Zhou, L.X., Zhang, C.L., Zhang, Y.Y., Liu, J.F., Fang, S.X., Yao, B., 2015. Summertime distributions of peroxyacetyl nitrate (PAN) and peroxypropionyl nitrate (PPN) in Beijing: understanding the sources and major sink of PAN. *Atmos. Environ.* 103, 289–296.